Accumulations of T-points in a model for solitary pulses in an excitable reaction-diffusion medium

Ale Jan Homburg
KdV Institute for Mathematics
University of Amsterdam
Plantage Muidergracht 24
1018 TV Amsterdam
The Netherlands
alejan@science.uva.nl

Mario A. Natiello*
Centre for Mathematical Sciences
Lund University
Sölvegatan 18
22100 Lund
Sweden
Mario.Natiello@math.lth.se

December 13, 2004

Abstract

We consider a family of differential equations that describes traveling waves in a reaction diffusion equation modeling oxidation of carbon oxide on a platinum surface, near the onset of spatio-temporal chaos. The organizing bifurcation for the bifurcation structure with small carbon oxide pressures, turns out to be a codimension three bifurcation involving a homoclinic orbit to an equilibrium undergoing a transcritical bifurcation. We show how infinitely many T-point bifurcations of multi loop heteroclinic cycles occur in the unfolding.

PACS: 05.45.+b; 47.20.Ky; 47.52.+j; 82.65.Jv
Keywords: Surface catalysis; Global bifurcation theory.

1 Introduction

We consider a set of differential equations describing traveling waves, and fronts and pulses, of a reaction diffusion system modeling the oxidation of CO on a Pt(110) surface. The purpose of this paper is to shed light on the structure of the global bifurcations relating to the behavior of pulses and fronts.

Let us briefly introduce the system. We refer to [1, 2, 3] for a deeper description of the model. Other papers discussing various aspects of the system include [4, 5, 6, 7, 8, 9, 10]. The FitzHugh-Nagumo type of

*To whom correspondence should be addressed.

partial differential equations are given by

$$\begin{aligned} \frac{\partial u}{\partial t} &= -\frac{1}{\varepsilon}u(u-1)(u-\frac{b+v}{a}) + \frac{\partial^2 u}{\partial x^2}, \\ \frac{\partial v}{\partial t} &= f(u) - v, \end{aligned}$$

with

$$f(u) = \begin{cases} 0, & 0 \le u < 1/3, \\ 1 - 27u(u-1)^2/4, & 1/3 \le u \le 1, \\ 1, & u > 1. \end{cases}$$

The parameters ε, b, a are physical parameters, related to pressures of oxide, carbon oxide and to temperature. The partial differential equations reduce to a system of ordinary differential equations when looking for traveling wave solutions:

$$\begin{aligned} \dot{u} &= w, \\ \dot{w} &= -cw + \frac{1}{\varepsilon}u(u-1)(u-\frac{b+v}{a}), \\ \dot{v} &= (v - f(u))/c, \end{aligned}$$

where c is the traveling wave speed. Pulses in the pde-system correspond to homoclinic loops in the ordinary differential equations. The three parameters that are varied are b, c, ε. The value of a is fixed (in [7] at 0.84).

For small values of b the bifurcation diagram in the (c, ε) plane contains two curves of homoclinic loops to hyperbolic equilibria $P = (0, 0, 0)$ and $Q = (b/a, 0, 0)$, that terminate in a heteroclinic bifurcation point. The homoclinic loops to Q correspond to pulses that are unstable. The homoclinic loops to P give stable pulses. The existence of homoclinic loops to P for ϵ sufficiently small can be proved by a straightforward application of the results in [11, 12]. These stable pulses disappear when ε is increased at the heteroclinic bifurcation point in what has been called a backfiring instability [5, 7, 9, 10]. The heteroclinic cycle consists of a codimension two connection from P to Q and a robust connection from Q to P, see Figure 1. Such heteroclinic bifurcation points, involving a robust and a codimension two connection between two equilibria, are known as T-points [13].

The two equilibria P, Q come together in a transcritical bifurcation at $b = 0$. Numerical computations [7, 8, 9] support our assumption of the existence of a particular organizing center in the bifurcation diagram. The organizing center, occurring at a point $(b, c, \varepsilon) = (0, c^*, \varepsilon^*)$ for some positive c^*, ε^*, consists of a transcritical bifurcation with a homoclinic orbit approaching the non-hyperbolic equilibrium along the normally hyperbolic directions. The bifurcation structure for small values of b can be uncovered from a bifurcation study of this organizing center. Doing so, we reveal the mechanisms in which multiple pulses are created.

We stress that we provide a bifurcation study not restricted to the particular system under consideration, but valid for any system (where we note that we make generic assumptions on eigenvalues) with a similar homoclinic loop to an equilibrium undergoing a saddle node or transcritical bifurcation.

The most interesting phenomenon we prove to exist is an infinite set of T-point bifurcations, involving the equilibria P and Q, the robust connection from Q to P and codimension two connections from P to Q of arbitrary arc length. To each finite sequence on two symbols there corresponds a T-point bifurcation. See

Figure 2 for a sketch of the bifurcation set and Section 5 (in particular Theorem 5.1) for the corresponding precise statements on the unfolding of the organizing center.

We acknowledge fruitful conversations with Hiroshi Kokubu. We gratefully acknowledge support from NWO, the Netherlands Organization for Scientific Research as well as from Vetenskapsrådet in Sweden.

2 Homoclinic loops and heteroclinic cycles

In this section we explain the geometry of the differential equations at and near the organizing center, with a homoclinic loop to a saddle-node equilibrium.

Under the assumption of non-resonance conditions among the eigenvalues [14], the normal form for a flow near a saddle-node in $\mathbb{R}^3$ is given by

$$\begin{aligned} \dot{x} &= \frac{x^2-\sigma}{1+kx}, \\ \dot{y} &= \lambda(x)y, \\ \dot{z} &= z. \end{aligned} \tag{1}$$

That is, in the absence of rational relations among the nonzero eigenvalues at the saddle-node equilibrium, a smooth coordinate change together with a smooth reparametrization of the time variable brings the vector field into the above expression. The adjective smooth stands for C^K for some sufficiently high unspecified integer K. Alternatively, one can write $\dot{x} = x^2 - kx^3$ for the equation in x, but the coefficient of the third order term cannot be altered, or removed, by smooth coordinate changes. Note that the computations in [8] were performed under the simplifying assumption $k = 0$. The function λ is negative. Note that λ depends on σ as well, but we do not make this explicit in the notation. We will in the sequel be concerned with the case $-\lambda(0) > 1$ for $\sigma = 0$, which is the relevant case for the numerical observations of reference [7]. We are interested in $\sigma \geq 0$ and write $\mu_1 = \sqrt{\sigma}$. This turns the local bifurcation into a transcritical bifurcation, consistent with the model.

Take two cross-sections $\Sigma^{in} = \{y = c_1\}$ and $\Sigma^{out} = \{z = c_2\}$, where c_1 and c_2 are suitable positive constants. By rescaling the y and z coordinates, we get $c_1 = 1$ and $c_2 = 1$. Let $\Psi^{loc} : \Sigma^{in} \to \Sigma^{out}$ be the local transition map. The transition time according to (1) is $t = -\ln z$. The first return map $\Psi^{glob} : \Sigma^{out} \to \Sigma^{in}$ is a local diffeomorphism which can be developed as

$$\Psi^{glob}(x,y) = \begin{pmatrix} \mu_2 \\ \mu_3 \end{pmatrix} + \begin{pmatrix} A & B \\ C & D \end{pmatrix} \begin{pmatrix} x \\ y \end{pmatrix} + h.o.t., \tag{2}$$

where the higher order terms are at least second order terms in (x, y). The Poincaré map $\Psi : \Sigma^{out} \to \Sigma^{out}$ is the composition $\Psi = \Psi^{loc} \circ \Psi^{glob}$. The two parameters μ_2, μ_3 describe global properties of the flow. Note that in reference [8] the role of A, C and B, D is interchanged because of the choice of coordinates.

The image of $\{y = 0\} \subset \Sigma^{out}$ by the global map will be a curve on Σ^{in}. The placement of the curve will depend on the values of (μ_2, μ_3). The inclination of the curve will depend on A and C. Numerical observations indicate that for the model,

$$C < 0 < A. \tag{3}$$

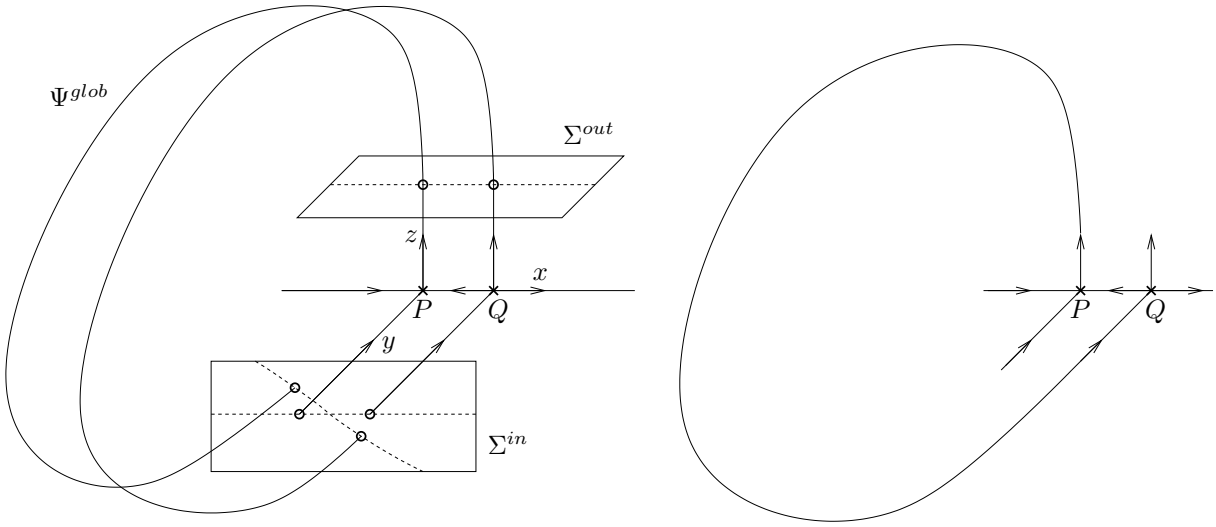

Figure 1: The return map for positive μ_1, in case $A > 0$ and $C < 0$. Depicted on the right is the codimension two heteroclinic cycle involving P and Q.
The consideration on orientability of stable and unstable manifolds of the equilibria at the T-point bifurcation, see [7], suggests $C < 0$. Further numerical experiments, not explicitely contained in [7, 8] but consisting of plotting images of transition maps, leads to the assumption (3).

With these sign conditions, the curve cuts the axis $\{z = 0\} \subset \Sigma^{in}$ transversally, crossing from top-left to bottom-right, compare Figure 1. The numerical observations that are commented upon but not explicitely contained in [7, 8], suggest this to be the case. We mention that considerations on orientability of stable and unstable manifolds of the equilibria at the T-point bifurcation in [7] imply $C < 0$. Although our analysis can be used for other sign conditions on A and C, and we do discuss some of the other possible cases where they are dynamically interesting, most of the bifurcation analysis in this paper concerns the case (3).

Consider $\mu_1 > 0$. Two equilibria, $P = (-\mu_1, 0, 0)$ and $Q = (\mu_1, 0, 0)$, exist. A homoclinic orbit to P occurs if $\Psi^{glob}(-\mu_1, 0) \in \{x < \mu_1, z = 0\}$. A homoclinic orbit to Q occurs if $(\mu_1, 0) \in \Psi^{glob}(\{x > -\mu_1, y = 0\})$. This yields two surfaces in the (μ_1, μ_2, μ_3) parameter space, bounded by a curve where $\Psi^{glob}(-\mu_1, 0) = (\mu_1, 0)$, which gives a heteroclinic cycle. The intersections of these bifurcation sets with a small sphere in the (μ_1, μ_2, μ_3) parameter space around the origin are depicted, in Figure 2, as the homoclinic bifurcation curves $\mathrm{Hom_P}$, $\mathrm{Hom_Q}$ and the heteroclinic bifurcation point $\mathrm{Het_{PQ}}$. At $\mathrm{Het_{PQ}}$, a heteroclinic cycle exists containing a codimension two connection from P to Q and a persistent connection from Q to P along the x-axis. The heteroclinic bifurcation $\mathrm{Het_{PQ}}$ was considered by V.V. Bykov [15], see also [13, 16].

Along the curves $\mathrm{Hom_Q}$, $\mathrm{Hom_P}$ there are codimension two orbit flip bifurcations. At $\mathrm{OF_P}$, the homoclinic

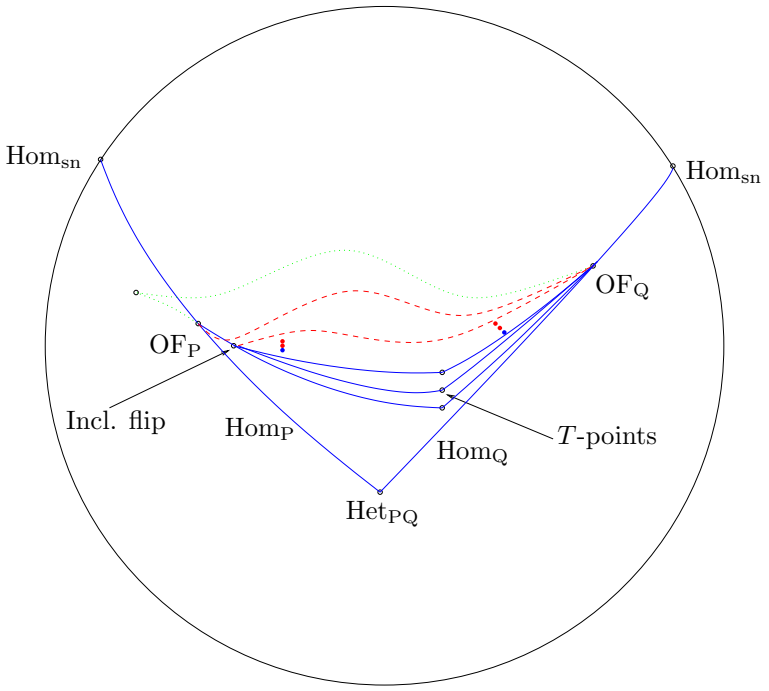

Figure 2: Sketch of the bifurcation set in case $A > 0, C < 0$, drawn on a half-sphere with $\mu_3 \geq 0$ around the origin in the (μ_1, μ_2, μ_3) parameter space. The circle is the intersection with $\mu_3 = 0$, for which the transcritical bifurcation occurs. Solid curves indicate homoclinic bifurcations, dashed curves are period doubling bifurcations and dotted curves are saddle node bifurcations of periodic orbits. Infinitely many inclination flips occur close to OF$_{\rm P}$ and infinitely many T-points occur close to the homoclinic bifurcation curve connecting Het$_{\rm PQ}$ and OF$_{\rm Q}$.

orbit to P approaches P along the strong stable direction, when time goes to infinity. Here $\Psi^{glob}(-\mu_1, 0) = (-\mu_1, 0)$. At OF$_{\rm Q}$, the homoclinic orbit to Q approaches Q along the strong unstable direction, for negative time. Here $\Psi^{glob}(\mu_1, 0) = (\mu_1, 0)$. Bifurcations of orbit flips were studied in [17, 18]. Summarizing: if $\lambda_1 < \lambda_2 < 0 < \lambda_3$ denote the eigenvalues at the equilibrium, then three possibilities occur. If $-\lambda_1 > -\lambda_2 > \lambda_3$ then no additional bifurcation curves branch from the orbit flip point. If $-\lambda_1 > \lambda_3 > -\lambda_2$, a homoclinic doubling bifurcation takes place where, in addition to curves of saddle node and period doubling bifurcations of periodic orbits, a curve of doubled homoclinic loops branches from the orbit flip point. The remaining case $\lambda_3 > -\lambda_1 > -\lambda_2$ shows curves of n-homoclinics for all n branching from the orbit flip point. At the point P, the eigenvalues of the linearized vector field are $\lambda(-\mu_1), -2\mu_1/(1 - k\mu_1)$ and 1. As $\lambda(-\mu_1) < -1$ and $-2\mu_1/(1 - k\mu_1)$ is small negative, a doubled homoclinic loop, and no other homoclinic loops, branches from OF$_{\rm P}$. Similarly one sees that near OF$_{\rm Q}$, there are infinitely many homoclinic loops, as well as infinitely many saddle node and period doubling bifurcation curves for periodic orbits. The sketch in Figure 2 indicates how the different bifurcation curves are connected, backed up by the analysis in the following sections.

The curves $\mathrm{Hom_P}$, $\mathrm{Hom_Q}$ end at $\mu_3 = 0$ at codimension two bifurcations indicated by $\mathrm{Hom_{sn}}$ in Figure 2, involving a saddle node equilibrium and a homoclinic loop to it. These bifurcations were studied in [19, 20]. These codimension two bifurcations involve a saddle-node equilibrium and a homoclinic loop that approaches it along the center direction and along a normally hyperbolic direction for large positive and negative times. The unfolding of these codimension two bifurcations involves only simple dynamics, and in fact only a single curve of homoclinic loops to a hyperbolic equilibrium is found to branch from the curve of saddle-node bifurcations. It is therefore remarkable that the codimension three bifurcation, where the homoclinic loop approaches the saddle-node equilibrium along the normally hyperbolic directions for large positive and negative times, can lead to complicated and new bifurcational phenomena.

3 Rescalings

We show how approximate interval maps are obtained from the return maps. The analysis of these interval maps, in the following section, reveals the intricate bifurcation structure sketched in Figure 2.

3.1 $\mu_1 = 0$

Recall the expression (1) for the local flow. For $\mu_1 = 0$, the equation in x integrates as

$$\frac{x(t)}{1 - kx(t)\ln|x(t)|} = \frac{x(0)}{1 - kx(0)\ln|x(0)| - x(0)t}.$$

Since $x \ln x < x^\omega$ for $0 < \omega < 1$, it follows that

$$x(t) = \frac{x(0)}{1 - kx(0)\ln|x(0)| - x(0)t} + \mathcal{O}\left(\frac{x(0)}{1 - kx(0)\ln|x(0)| - x(0)t}\right)^{1+\omega}, \tag{4}$$

for $0 < \omega < 1$. For the y coordinate, one has

$$y(t) = e^{\int_0^t \lambda(x(s))ds}. \tag{5}$$

Since $\lambda(x) = \lambda(0) + \mathcal{O}(x)$, computing $e^{\int_0^t \mathcal{O}(x(s))ds}$ one realizes that $y(t)$ is dominated by $e^{-\tilde{\nu}t}$ for some $\tilde{\nu}$ close to $-\lambda(0) = \nu$ for t large enough:

$$y(t) \leq Ce^{-\tilde{\nu}t}, \tag{6}$$

for some $C > 0$.

Take ξ with $1 < \xi < \tilde{\nu}$. For $\mu_2 \neq 0$, consider the following rescaled coordinates,

$$\begin{aligned} |\mu_2|\bar{x} &= x, \\ |\mu_2|^\xi \bar{y} &= y, \end{aligned}$$

and define $|\mu_2|\bar{\mu}_3 = \mu_3$. One considers values of x, y, μ_3 so that $|\bar{x}|, |\bar{y}|, |\bar{\mu}_3|$ are bounded (so μ_3 is restricted to be of the order of μ_2).

Lemma 3.1 *Let $\bar{\Psi}$ be the return map in the rescaled coordinates $(\bar{x}, \bar{y})$. In the limit $\mu_2 \to 0$, one can write*

$$\bar{\Psi}(\bar{x}, \bar{y}) \quad = \quad \begin{pmatrix} \frac{\mathrm{sgn}(\mu_2)+A\bar{x}}{1+|\mu_2|(\mathrm{sgn}(\mu_2)+A\bar{x})\ln(\bar{\mu}_3+C\bar{x})} \\ 0 \end{pmatrix}.$$

Remark 3.2 *Note that a term containing μ_2 is retained, because its factor is large if $\bar{\mu}_3 + C\bar{x}$ is small. The convergence is uniform only away from $\bar{x}$ with $\bar{\mu}_3 + C\bar{x} = 0$. Away from $\bar{x} = -\bar{\mu}_3/C$, the first coordinate of $\bar{\Psi}$ converges uniformly to $\bar{x} \mapsto \mathrm{sgn}(\mu_2) + A\bar{x}$.*

Proof. Take $(x, y) \in \Sigma^{out}$. Composing (2) with (4), (5) for $t = -\ln z$ gives the return map $(x, y) \mapsto \Psi(x, y)$. Further, the rescaling is given by a map $h(x, y) = (|\mu_2|x, |\mu_2|^{\xi}y)$. A direct computation of $\bar{\Psi} = h^{-1} \circ \Psi \circ h$ gives, after taking the limit $\mu_2 \to 0$, the asymptotic form for the return map in the rescaled coordinates. □

Another set of rescaled coordinates, for $\mu_3 \neq 0$, is given by

$$\begin{aligned} |\mu_3|\hat{x} &= x, \\ |\mu_3|^{\xi}\hat{y} &= y. \end{aligned}$$

Here one introduces $|\mu_3|\hat{\mu_2} = \mu_2$. One considers values of x, y, μ_2 so that $|\hat{x}|, |\hat{y}|, |\hat{\mu_2}|$ are bounded (hence μ_2 is required to be of the order of μ_3).

Lemma 3.3 *Let $\hat{\Psi}$ be the return map in the rescaled coordinates $(\hat{x}, \hat{y})$. In the limit $\mu_3 \to 0$, one can write*

$$\hat{\Psi}(\hat{x}, \hat{y}) \quad = \quad \begin{pmatrix} \frac{\hat{\mu}_2+A\hat{x}}{1+|\mu_3|(\hat{\mu}_2+A\hat{x})\ln(\mathrm{sgn}(\mu_3)+C\hat{x})} \\ 0 \end{pmatrix}.$$

Note that now a term multiplying μ_3 is retained. Away from $\hat{x} = -\mathrm{sgn}(\mu_3)/C$, the first coordinate of $\hat{\Psi}$ converges uniformly to $\hat{x} \mapsto \hat{\mu}_2 + A\hat{x}$. The two rescalings together cover all small values of μ_2 and μ_3, $(\mu_2, \mu_3) \neq (0, 0)$.

3.2 $\mu_1 > 0$

For $\mu_1 > 0$, two equilibria $P = (-\mu_1, 0, 0)$ and $Q = (\mu_1, 0, 0)$ exist. We are interested in understanding the details of the dynamics in a region with x coordinate containing the interval $[-\mu_1, \mu_1]$, which is relevant for nonzero μ_1. It is convenient to rescale $\bar{x}\mu_1 = x$. Multiplying the differential equation for $\bar{x}$ with a factor $1/\mu_1$ (or rescaling time by this factor) yields the differential equation

$$\dot{\bar{x}} = (\bar{x}^2 - 1)/(1 + k\mu_1\bar{x}). \tag{7}$$

Note that for bounded $\bar{x}$ the differential equation converges to $\dot{\bar{x}} = \bar{x}^2 - 1$ as $\mu_1 \to 0$. The differential equation (7) is solved by

$$\frac{(1 - \bar{x}(t))^{1+k\mu_1}}{(1 + \bar{x}(t))^{1-k\mu_1}} = e^{2t}\frac{(1 - \bar{x}(0))^{1+k\mu_1}}{(1 + \bar{x}(0))^{1-k\mu_1}}. \tag{8}$$

This defines $\bar{x}(t)$ as a smooth function of $\bar{x}(0), t$ and μ_1, for μ_1 close to 0. This is clear away from $\bar{x}(0) = \pm 1$ and $\mu_1 = 0$. If e.g. $\bar{x}(0) = -1$ and $\mu_1 = 0$, after taking the $\frac{1}{1-k\mu_1}$-th power of the equation, smoothness follows from the implicit function theorem. Recall that $\bar{y}(t)$ is given by

$$y(t) \quad = \quad e^{\int_0^t \lambda(x(s))ds}. \tag{9}$$

For the return map $(x, y) \mapsto \Psi(x, y)$, we scale $x = \mu_1 \bar{x}$ as above and $y = \mu_1^{\xi} \bar{y}$, with $1 < \xi < \tilde{\nu}$. Rename μ_2 and μ_3 as $\mu_1\bar{\mu}_2$, $\mu_1\bar{\mu}_3$.

Lemma 3.4 *Let $\bar{\Psi}$ be the return map in the rescaled coordinates $(\bar{x}, \bar{y})$. In the limit $\mu_1 \to 0$, one can write*

$$\bar{\Psi}(\bar{x}, \bar{y}) \quad = \quad \begin{pmatrix} \frac{(\bar{\mu}_3 + C\bar{x})^{2\mu_1} - \frac{1-(\bar{\mu}_2 + A\bar{x})}{1+\bar{\mu}_2 + A\bar{x}}}{(\bar{\mu}_3 + C\bar{x})^{2\mu_1} + \frac{1-(\bar{\mu}_2 + A\bar{x})}{1+\bar{\mu}_2 + A\bar{x}}} \\ 0 \end{pmatrix}. \tag{10}$$

Remark 3.5 *The term $(\bar{\mu}_3 + C\bar{x})^{2\mu_1}$ containing μ_1 is kept in the limit map, since this equals 1 for $\mu_1 = 0$ except at $\bar{x} = -\bar{\mu}_3/C$ where $\bar{\mu}_3 + C\bar{x} = 0$. The convergence is uniform only away from $\bar{x} = -\bar{\mu}_3/C$. Away from $\bar{x} = -\bar{\mu}_3/C$, the first coordinate of the return map converges to the affine map*

$$\bar{x} \mapsto \frac{1 - \frac{1-(\bar{\mu}_2 + A\bar{x})}{1+\bar{\mu}_2 + A\bar{x}}}{1 + \frac{1-(\bar{\mu}_2 + A\bar{x})}{1+\bar{\mu}_2 + A\bar{x}}} = \bar{\mu}_2 + A\bar{x}. \tag{11}$$

Proof. Consider first $k = 0$ in (1). The local flow for (7) is then given by

$$\bar{x}(t) = \frac{e^{-2t} + \frac{\bar{x}(0)-1}{\bar{x}(0)+1}}{e^{-2t} - \frac{\bar{x}(0)-1}{\bar{x}(0)+1}}, \tag{12}$$

where $t = -\mu_1 \ln z$ and $z = \mu_3 + Cx + Dy = \mu_1\bar{\mu}_3 + C\mu_1\bar{x} + D\mu_1^{\xi}\bar{y}$. Combining this with (2) gives asymptotics for the rescaled return map.

Now suppose $k \neq 0$ in (7) and let $\zeta = k\mu_1$. Denote $s = e^{-2t}$. The local flow for (7) satisfies

$$s(\bar{x}(t) - 1)^{1+\zeta}(\bar{x}(0) + 1)^{1-\zeta} = (\bar{x}(t) + 1)^{1-\zeta}(\bar{x}(0) - 1)^{1+\zeta}.$$

As remarked before, for $s \neq 0$, this gives $\bar{x}(t)$ as a smooth function of $\bar{x}(0), s, \zeta$. Note that $\bar{x}(t) = -1$ if $s = 0$. Taking the $\frac{1}{1-\zeta}$-th power of this equation and letting $u = s^{1/(1-\zeta)}$, we get

$$u(\bar{x}(t) - 1)^{(1+\zeta)/(1-\zeta)}(\bar{x}(0) + 1) = (\bar{x}(t) + 1)(\bar{x}(0) - 1)^{(1+\zeta)/(1-\zeta)}.$$

If $\bar{x}(0)$ and $\bar{x}(t)$ are away from 1, the implicit function theorem lets us solve $\bar{x}(t)$ depending smoothly on $u, \bar{x}(0), \zeta$. The solution therefore converges to the solution for $k = 0$, as $\mu_1 \to 0$.

Combined with (2) this shows the following. Away from $\bar{x} = -\bar{\mu}_3/C$, the return map converges to the affine map $\bar{x} \mapsto \bar{\mu}_2 + A\bar{x}$ as $\mu_1 \to 0$. And, assuming that $\bar{\mu}_2 + A\bar{x} \neq \pm 1$ at $\bar{x} = -\bar{\mu}_3/C$, convergence to (10) holds also near $\bar{x} = -\bar{\mu}_3/C$. □

Let $\mathcal{C} = \left(\Psi^{glob}\right)^{-1}(\{z=0\})$ and $\bar{\mathcal{C}}$ the same in rescaled coordinates. Note that $\bar{\mathcal{C}}$ is close to the line of constant $\bar{x}$ coordinate $\bar{x}_r = -\bar{\mu}_3/C$. The rescaled return map $\bar{\Psi}$ is defined only on one side of $\bar{\mathcal{C}}$.

For later use we indicate how estimates on partial derivatives of $\bar{\Psi}$ for μ_1 small are obtained. These are straightforward to obtain using estimates on derivatives of $x(t)$ and $y(t)$ from (8) and (9) for $t = -\mu_1 \ln z$. With $\bar{x}_0 = \bar{x}(0)$ and $\bar{x}_1 = \bar{x}(t)$ at $t = -\mu_1 \ln z$, we get $\bar{x}_1$ as function of $\bar{x}_0$ and z. Differentiating (8) yields

$$\frac{\partial \bar{x}_1}{\partial \bar{x}_0}\frac{\partial}{\partial \bar{x}_1}\left(\frac{(1-\bar{x}_1)^{1+\zeta}}{(1+\bar{x}_1)^{1-\zeta}}\right) = z^{-2\mu_1}\frac{\partial}{\partial \bar{x}_0}\left(\frac{(1-\bar{x}_0)^{1+\zeta}}{(1+\bar{x}_0)^{1-\zeta}}\right)$$

from which one obtains (after some manipulation using (8) which allows for rewriting to equivalent forms)

$$\frac{\partial \bar{x}_1}{\partial \bar{x}_0} = z^{-2\mu_1/(1+\zeta)}\left(\frac{1+\bar{x}_1}{1+\bar{x}_0}\right)^{2/(1+\zeta)}\frac{1+\zeta\bar{x}_0}{1+\zeta\bar{x}_1}. \tag{13}$$

Similarly,

$$\frac{\partial \bar{x}_1}{\partial z}\frac{\partial}{\partial \bar{x}_1}\left(\frac{(1-\bar{x}_1)^{1+\zeta}}{(1+\bar{x}_1)^{1-\zeta}}\right) = -2\mu_1 z^{-2\mu_1-1}\frac{(1-\bar{x}_0)^{1+\zeta}}{(1+\bar{x}_0)^{1-\zeta}}$$

from which one gets

$$\frac{\partial \bar{x}_1}{\partial z} = \mu_1\frac{1}{z}\frac{(1+\bar{x}_1)(1-\bar{x}_1)}{1+\zeta\bar{x}_1}. \tag{14}$$

Formulas (13) and (14) with (8) enable an estimate of the derivatives $\frac{\partial \bar{x}_1}{\partial \bar{x}_0}$ and $\frac{\partial \bar{x}_1}{\partial z}$ for small μ_1 when also ζ is small. Analogously,

$$\frac{\partial y}{\partial \bar{x}_0} = e^{\int_0^t \lambda(\mu_1\bar{x}(s))ds}\int_0^t \mu_1\lambda'(\mu_1\bar{x}(s))\frac{\partial \bar{x}(s)}{\partial \bar{x}_0}ds$$

and

$$\frac{\partial y}{\partial z} = -\mu_1 e^{\int_0^t \lambda(\mu_1\bar{x}(s))ds}\frac{1}{z}\lambda(\mu_1\bar{x}_1),$$

from which one estimates $\frac{\partial y}{\partial \bar{x}_0}$ and $\frac{\partial y}{\partial z}$.

The computations show for instance that away from $\bar{\mathcal{C}}$ (i.e. away from $\bar{x} = -\bar{\mu}_3/C$ for small μ_1), $\frac{\partial}{\partial \bar{x}}\bar{\Psi}(\bar{x},\bar{y}) \to (A,0)$ and $\frac{\partial}{\partial \bar{y}}\bar{\Psi}(\bar{x},\bar{y}) \to (0,0)$ as $\mu_1 \to 0$. We indicate how an estimate on $D\bar{\Psi}(\bar{x},\bar{y})$ as $(\bar{x},\bar{y}) \to \bar{\mathcal{C}}$ is obtained. Suppose the positive orbit of the flow starting at $(\bar{x},\bar{y})$ intersects Σ^{in} in a point with rescaled x coordinate $\bar{x}_0$ and z coordinate z, such that $\bar{x}_0 \in (-1,1)$ and $z > 0$ small. If $\bar{x}_0$ is strictly away from -1, then $1+\bar{x}_1 \geq kz^{-2\mu_1/(1-\eta)}$ for some $k > 0$. If further $\bar{x}_1$ (the x coordinate of $\bar{\Psi}(\bar{x},\bar{y})$) is strictly away from 1, then $\frac{\partial \bar{x}_1}{\partial z} \geq k\mu_1 z^{-1+2\mu_1/(1-\zeta)}$ for some $k > 0$. With similar estimates for the other derivatives this implies that under these conditions the x coordinate of $\frac{\partial}{\partial \bar{x}}\bar{\Psi}(\bar{x},\bar{y})$ diverges as $(\bar{x},\bar{y}) \to \bar{\mathcal{C}}$.

4 Analysis of the interval maps

As shown above, for $\mu_1 = 0$ as well as for $\mu_1 > 0$, we have an interval map roughly describing the overall dynamics. The map depends on the parameters μ_1, μ_2, μ_3 and also on the coefficients A and C of the global map. In this section we will discuss bifurcations of the intervals maps, thereby using terminology suggested by the interpretation for the differential equations.

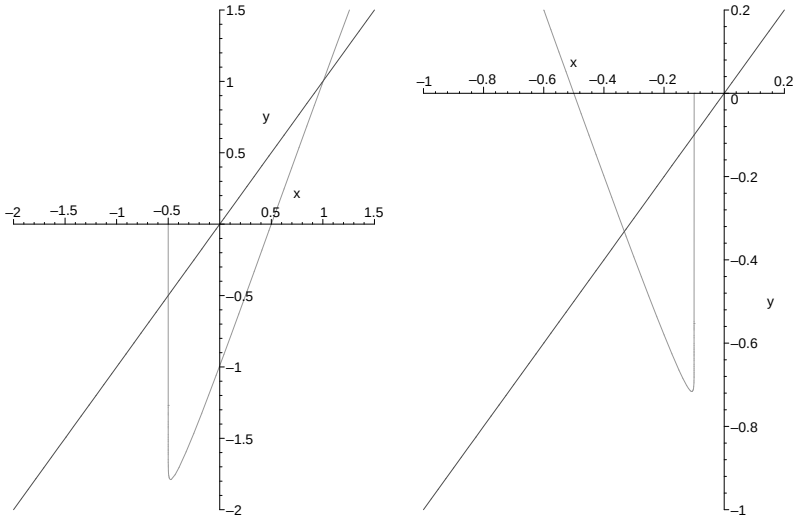

a) $A, C > 0, \mu_2 < 0 < \mu_3$, b) $A, C < 0, \mu_2, \mu_3 < 0$

Figure 3: Graphs of the interval maps for $\mu_1 = 0$. Pictures assume $|A| > 1$.

4.1 $\mu_1 = 0$

We have $f(\bar{x}) = \frac{\text{sgn}(\mu_2)+A\bar{x}}{1-\mu_2(\text{sgn}(\mu_2)+A\bar{x})\ln(\bar{\mu}_3+C\bar{x})}$ with $|\mu_2|\bar{\mu}_3 = \mu_3$. Provided μ_2 is small and $\text{sgn}(\mu_2) + A\bar{x} < 0$ at $\bar{x} = -\bar{\mu}_3/C$, the denominator in f is never zero in the natural domain of definition for f (i.e., $\bar{\mu}_3 + C\bar{x} > 0$). Indeed, for values of $\bar{x}$ such that $\bar{\mu}_3 + C\bar{x}$ is away from zero, $f(\bar{x})$ will behave roughly as the linear function $\bar{x} \mapsto \text{sgn}(\mu_2) + A\bar{x}$ if μ_2 is sufficiently small. When $\bar{x}$ approaches $-\bar{\mu}_3/C$, $f(\bar{x})$ will bend approaching zero with infinite slope, since the denominator goes to ∞. If $\text{sgn}(\mu_2) + A\bar{x} > 0$ at $\bar{x} = -\bar{\mu}_3/C$, f diverges to plus or minus ∞ close to $\bar{x} = -\bar{\mu}_3/C$. If A, C have the same sign, the above conditions hold for $\bar{\mu}_3 > \text{sgn}(\mu_2)C/A$. The graph of f is then unimodal. If A, C have opposite signs, one does not obtain a unimodal graph for f.

Define the line in the parameter plane $\mathcal{D} = \{\mu_2 = \mu_3(A-1)/C, \mu_3 < 0)\}$.

Lemma 4.1 *Suppose $A > 0, C > 0$. Parameters along the μ_2 axis correspond to homoclinic bifurcations to the saddle-node fixed point. Non-hyperbolic periodic orbits occur for parameters near $\mathcal{D}$.*

Proof. The line $\mu_3 = 0$ is clearly in the bifurcation set. Bifurcations of periodic orbits occur near parameter values where the critical point is fixed. That is, if $\bar{x} \mapsto \text{sgn}(\mu_2) + A\bar{x}$ intersects the diagonal near $\bar{x} = -\bar{\mu}_3/C$. This happens near the line $\bar{\mu}_3 = \text{sgn}(\mu_2)\text{C}/(\text{A}-1)$, that is, near $\mathcal{D}$. □

Homoclinic orbits to the saddle-node equilibrium correspond to points $\bar{x} > 0$ with $f^i(\bar{x}) = -\bar{\mu}_3/C$ for some $i \geq 1$. Assume that $A > 1$. Then there is a fixed point p for f, with $p \to \text{sgn}(\mu_2)/(1-A)$ as $\mu_2 \to 0$. See Figure 3a) for an illustration. For $A > 1$ and $\mu_2 > 0$ one can find the persistent occurrence, for the interval map, of infinitely many homoclinic orbits. The fixed point of the interval map corresponds to a

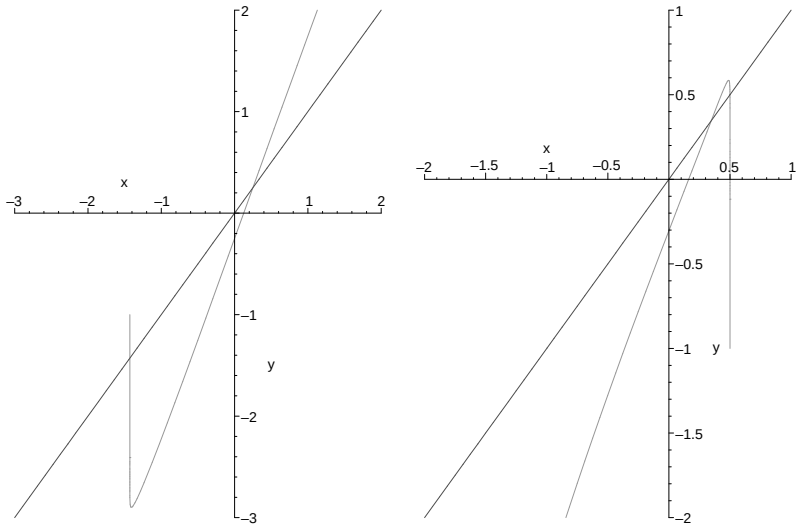

a) $A, C > 0, \mu_2 < 0 < \mu_3$ b) $C < 0 < A, \mu_2 < 0 < \mu_3$

Figure 4: Interval maps for $\mu_1 > 0$. Pictures assume $A > 1$.

saddle periodic orbit for the vector field. Its unstable manifold intersects the stable manifold of the saddle node equilibrium, whereas the unstable manifold of the saddle node equilibrium intersects the stable manifold of the periodic orbit (for the interval map this translates to iterates of points slightly larger than $-\bar{\mu}_3/C$ eventually hitting p).

4.2 $\mu_1 > 0$

The system in study has some interesting additional structure which is only present for positive μ_1. Fix $\mu_1 > 0$ and consider the obtained interval map

$$f(\bar{x}) = \frac{(\bar{\mu}_3 + C\bar{x})^{2\mu_1} - \frac{1-(\bar{\mu}_2+A\bar{x})}{1+\bar{\mu}_2+A\bar{x}}}{(\bar{\mu}_3 + C\bar{x})^{2\mu_1} + \frac{1-(\bar{\mu}_2+A\bar{x})}{1+\bar{\mu}_2+A\bar{x}}}, \tag{15}$$

in the appropriate scaled coordinates, for $A > 0 > C$ and depending on parameters $\bar{\mu}_2$, $\bar{\mu}_3$ (recall that $\bar{\mu}_2\mu_1 = \mu_2$, $\bar{\mu}_3\mu_1 = \mu_3$). When the global map hits the line $z = 0$ then the local map drives the corresponding $\bar{x}$ value to -1 except when the value of $\bar{x}$ is exactly the one corresponding to the stable manifold of $+1$. In order to let f comply with these constraints we let $f(-\bar{\mu}_3/C) = +1$ if $\bar{\mu}_2 + A\bar{x} = 1$. Note that $f(-\bar{\mu}_3/C) = -1$ if $\bar{\mu}_2 + A\bar{x} < 1$.

For arbitrarily small μ_1, the term $(\bar{\mu}_3 + C\bar{x})^{2\mu_1}$ will be essentially unity, unless $\bar{\mu}_3 + C\bar{x}$ is too close to zero. Hence, for most values of $\bar{x}$, f will approximately behave as $\bar{x} \mapsto \bar{\mu}_2 + A\bar{x}$. When $\bar{\mu}_3 + C\bar{x}$ approaches zero, $f(\bar{x})$ approaches -1 with infinite slope. See Figure 4 for an illustration.

Suppose then that $\bar{\mu}_3 + C\bar{x}_1 = 0$ for some $\bar{x}_1 \in [-1, 1]$. Further let $X_1 = \bar{\mu}_2 + A\bar{x}_1 \in [-1, 1]$ for the same value $\bar{x}_1$. If this holds for $\bar{x}_1 = -X_1 = -1$ we have a heteroclinic loop connecting the fixed points at $\bar{x} = -1$ and $\bar{x} = +1$. If $-1 < \bar{x}_1 \leq X_1 = 1$ we have then a 1-parameter curve of homoclinic loops at $\bar{x} = +1$. Similarly if $-1 = \bar{x}_1 \leq X_1 < 1$ there is a 1-parameter curve of homoclinic loops at $\bar{x} = -1$.

4.3 Orbit flip results for the case $A > 0 > C$.

We summarize the discussion for $A > 0$ and $C < 0$.

- A homoclinic orbit to -1 occurs if $\bar{\mu}_3 + C\bar{x} = 0$ and $\bar{\mu}_2 + A\bar{x} < 1$ for $\bar{x} = -1$, i.e. on the line $\mathcal{H}_{-1} = \{(\bar{\mu}_2 < 1 + A, \bar{\mu}_3 = C)\}$ in the parameter plane. An orbit flip occurs if moreover $\bar{\mu}_2 + A(-1) = -1$, thus at $O_{-1} = (A - 1, C)$. This orbit flip is a homoclinic doubling bifurcation [18, 17, 21].
- A homoclinic orbit to 1 occurs if $\bar{\mu}_2 + A\bar{x} = 1$ for $\bar{x} = -\bar{\mu}_3/C$ so that $\bar{x} > -1$. This yields the line $\mathcal{H}_1 = \{(\bar{\mu}_2 = 1 + A\bar{\mu}_3/C, \bar{\mu}_3 > C)\}$ in the parameter plane. An orbit flip occurs if also $-\bar{\mu}_3/C = 1$. This gives the point $O_1 = (1 - A, -C)$. Infinitely many curves of homoclinic bifurcations branch from this point [18, 17].
- A heteroclinic bifurcation or T-point occurs at the mutual end point of $\mathcal{H}_{-1} \cap \mathcal{H}_1 = (1 + A, C)$. The homoclinic orbits that branch from this point are twisted [17].

The last item is clear since the two half-lines with homoclinic orbits to both equilibria terminate at a point $(\bar{\mu}_2, \bar{\mu}_3) = (1 + A, C)$. This corresponds to a heteroclinic bifurcation. Let $\mathcal{D}$ denote the line in the parameter plane connecting the points O_{-1} and O_1 on which the line $\bar{x} \mapsto \bar{\mu}_2 + A\bar{x}$ intersects the diagonal at $\bar{x} = -\bar{\mu}_3/C$: $\mathcal{D} = \{(\bar{\mu}_2 = -\bar{\mu}_3(1 - A)/C, C < \bar{\mu}_3 < -C)\}$. Define the line $\mathcal{H}_\infty$ with constant $\bar{\mu}_2$ coordinate that extends between the orbit flip point O_{-1} and $\mathcal{H}_1$: $\mathcal{H}_\infty = \{(\bar{\mu}_2 = -1 + A, C < \bar{\mu}_3 < (-2 + A)C/A)\}$. For parameter values on this line, $\bar{x} = -1$ is a fixed point of $\bar{x} \mapsto \bar{\mu}_2 + A\bar{x}$. Write $g(\bar{x}) = \bar{\mu}_2 + A\bar{x}$ and define the line $\mathcal{H}_k$ connecting $\mathcal{H}_{-1}$ with $\mathcal{H}_1$, on which $g^{k-1}(-1) = -\bar{\mu}_3/C$. In the limit $\mu_1 = 0$, this corresponds to k-homoclinic loops to the point -1. The line $\mathcal{H}_k$ lies on $\bar{\mu}_2(1 + \ldots + A^{k-2}) - A^{k-1} = -\bar{\mu}_3/C$.

Lemma 4.2 *Suppose $A > 1, C < 0$. As $\mu_1 \downarrow 0$, the line $\mathcal{D}$ is the limit of bifurcations of non-hyperbolic periodic orbits, while the loci of homoclinic and heteroclinic bifurcations, converge to $\mathcal{H}_{-1} \cup \mathcal{H}_1 \cup \mathcal{H}_2 \cup \mathcal{H}_3 \cup \ldots \cup \mathcal{H}_\infty$.*

PROOF. The graph of f is unimodal for parameter values inside the region bounded by $\mathcal{H}_{-1}$ and $\mathcal{H}_1$. As $\mu_1 \downarrow 0$, the graph of f converges to the union of a line $\bar{\mu}_2 + A\bar{x}, \bar{x} < -\bar{\mu}_3/C$ and a vertical line at $\bar{x} = -\bar{\mu}_3/C$. Notice that for parameter values away from $\mathcal{D}$, intersections of f with the diagonal have slope either close to $A > 1$ or large negative. It follows that bifurcations involving non-hyperbolicity of orbits, such as saddle-node and period-doubling bifurcations of periodic orbits, occur only near $\mathcal{D}$. Possible remaining bifurcations, in particular homoclinic and heteroclinic bifurcations, involve the points -1 and 1. Due to the large negative slope of f as $\bar{x}$ approaches $-\bar{\mu}_3/C$, these bifurcations accumulate onto $\mathcal{H}_{-1} \cup \mathcal{H}_1 \cup \mathcal{H}_2 \cup \mathcal{H}_3 \cup \ldots \cup \mathcal{H}_\infty$ as $\mu_1 \downarrow 0$. □

For $0 < A < 1$, the lines $\mathcal{H}_{-1}$ and $\mathcal{H}_1$, as well as the points O_{-1}, O_1, T, are as above. Write $g(\bar{x}) = \bar{\mu}_2 + A\bar{x}$. Let $\mathcal{H}_k$ be the set of parameters on the line piece between $\mathcal{H}_{-1}$ and $\mathcal{H}_1$, for which $g^{k-1}(-1) = -\bar{\mu}_3/C$.

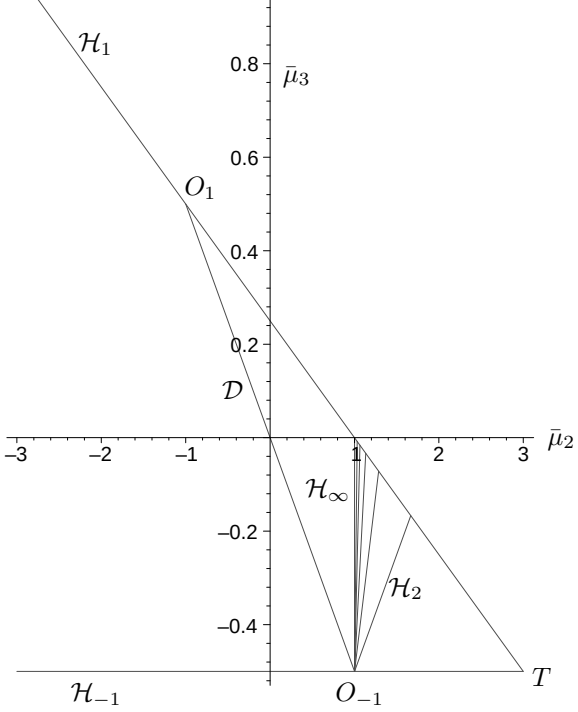

Figure 5: Take $A > 1, C < 0$. The limit of the bifurcation set in the $\bar{\mu}_2, \bar{\mu}_3$ parameter plane, as $\mu_1 \downarrow 0$, of the interval map f consists of two line segments where -1 and 1 are fixed points and countable many line segments connecting between these two.

Again this correpsonds, in the limit $\mu_1 = 0$, to k-homoclinic loops to -1. Let $\mathcal{D}$ be the parameters satisfying $g(-\bar{\mu}_3/C) = -\bar{\mu}_3/C$.

Lemma 4.3 *Suppose $0 < A < 1, C < 0$. As $\mu_1 \downarrow 0$, the bifurcation set of f converges to a union of line pieces $\mathcal{H}_{-1} \cup \mathcal{H}_1 \cup \mathcal{D} \cup \mathcal{H}_2 \cup \ldots$. The line $\mathcal{D}$ is the limit of bifurcations involving non-hyperbolic periodic orbits. Homoclinic and heteroclinic bifurcations, in the limit $\mu_1 \downarrow 0$, are contained in $\mathcal{H}_{-1} \cup \mathcal{H}_1 \cup \mathcal{H}_2 \cup \mathcal{H}_3 \cup \ldots$.*

5 Accumulations of heteroclinic bifurcations

The result below makes clear the complexity of the bifurcation diagram when μ_2 and μ_3 are varied and μ_1 is fixed. It will follow from the arguments that at least generically, there are infinitely many curves formed by homoclinic loops to P, where each of these curves terminates at a T-point. Let $\bar{\mu}_2, \bar{\mu}_3$ be rescaled parameters, rescaled by $1/\mu_1$, as in Lemma 3.4.

The proof of the following theorem will follow from a series of lemma's in this section. The theorem supposes $A > 1$, the case $0 < A < 1$ is discussed at the end of the section.

Theorem 5.1 *Suppose $A > 1, C < 0$. Consider two parameter families $\dot{x} = X_{\bar{\mu}_2, \bar{\mu}_3}(x)$ for fixed values of $\mu_1 > 0$. For all $\mu_1 > 0$ sufficiently small, there are infinitely many T-point bifurcations accumulating onto $\mathcal{H}_1$ as $\mu_1 \to 0$. There are infinitely many inclination flips of homoclinic loops to P accumulating onto O_{-1} as $\mu_1 \to 0$.*

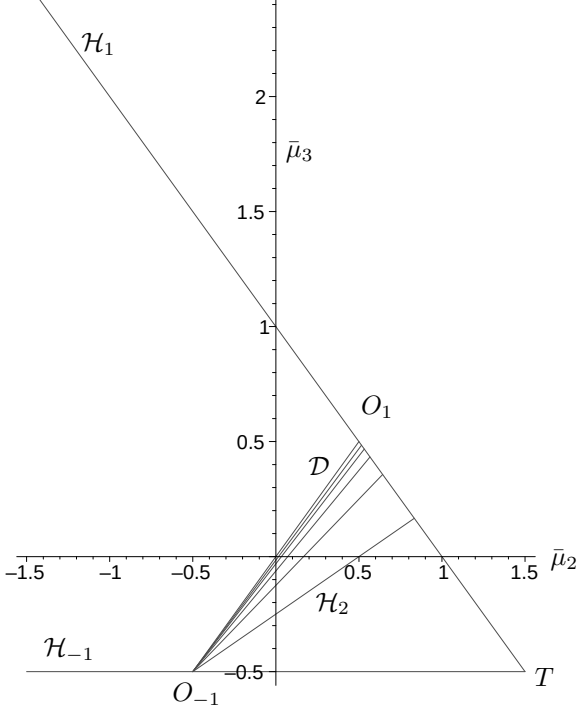

Figure 6: Take $0 < A < 1, C < 0$. The limit of the bifurcation set in the $\bar{\mu}_2, \bar{\mu}_3$ parameter plane , as $\mu_1 \downarrow 0$, of the interval map f consists of two line segments where -1 and 1 are fixed points and countable many line segments connecting between these two.

The strategy to prove this theorem consists of pathfollowing curves of homoclinic bifurcations (of homoclinic loops to P), using the general continuation theory in [21] to describe the possibilities in which the pathfollowing is terminated, and developing analysis particular to the case to rule out several of the possibilities. This will show that the pathfollowing of curves of homoclinic loops to P terminates at T-points.

Consider $\dot{x} = X_{\bar{\mu}_2,\bar{\mu}_3}(x)$ for small fixed values of $\mu_1 > 0$. We first rule out the occurrence of orbit flip bifurcations of n-homoclinic loops to P for $n > 1$. For small μ_1 there are curves of homoclinic bifurcations close to the line pieces $\mathcal{H}_{-1}$ and $\mathcal{H}_1$. We write $\mathcal{H}_{-1}(\mu_1)$ and $\mathcal{H}_1(\mu_1)$ for these curves, joining at a T-point bifurcation.

Lemma 5.2 *Suppose $C < 0 < A$. For small $\mu_1 > 0$, there are no orbit flip homoclinic bifurcations of n-homoclinic loops to P with $n > 1$, in the region bounded by $\mathcal{H}_{-1}(\mu_1)$ and $\mathcal{H}_1(\mu_1)$.*

Proof. An orbit flip of an n-homoclinic loop occurs if $\Psi^{glob} \circ \Psi^{n-1}(-\mu_1, 0) = (-\mu_1, 0)$. Since Ψ^{glob} is orientation preserving, it maps a strip $\{0 \le y < y^*\} \subset \Sigma^{out}$ to the right (i.e. with larger values of x) of the curve $\Psi^{glob}(\{y = 0\})$. The curve $\Psi^{glob}(\{y = 0\})$ intersects the x-axis (in the stable manifold of P) in a point Z depending on the parameters.

For parameters in the region bounded by $\mathcal{H}_{-1}$ and $\mathcal{H}_1$, one has $Z > -\mu_1$. Then $(-\mu_1, 0)$ lies outside the image under Ψ^{glob} of the strip $\{0 \le y < y^*\} \subset \Sigma^{out}$. It is therefore clear that orbit flips cannot occur. See Figure 7 for an illustration.

Of course $\Psi^{glob}(-\mu_1, 0) = (Z, 0)$ for $Z < -\mu_1$ corresponds to the curve of single homoclinic loops to P,

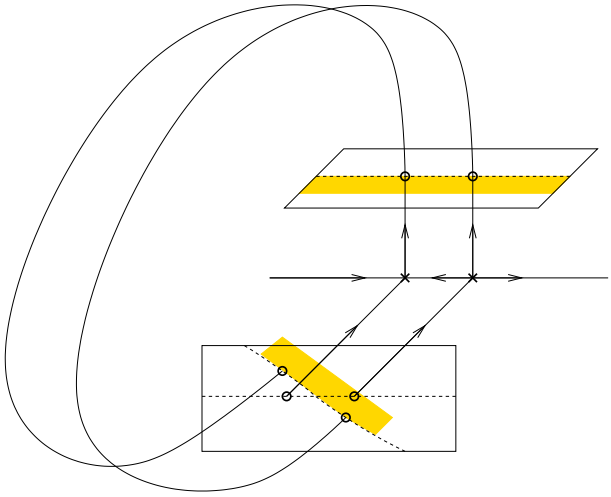

Figure 7: This picture illustrates the reasoning to show that orbit flips of n-homoclinic loops to P with $n > 1$, do not occur for parameters from the wedge between $\mathcal{H}_{-1}(\mu_1)$ and $\mathcal{H}_1(\mu_1)$.

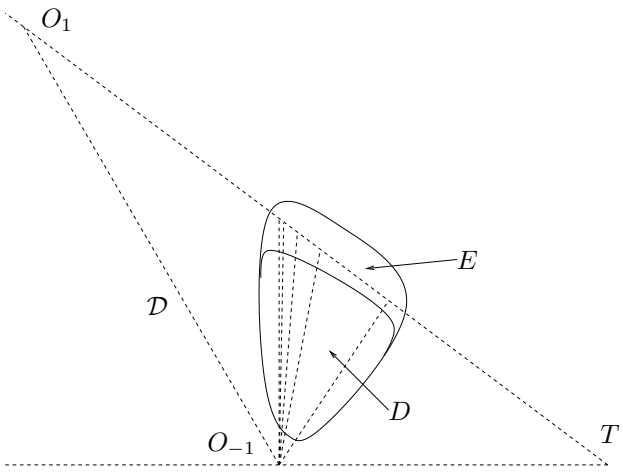

Figure 8: T-points are sought for in a region E in the $(\bar{\mu}_2, \bar{\mu}_3)$ parameter plane. The rescaled return map admits a stable foliation for parameters from a slightly smaller region D, which does not include $\mathcal{H}_1$.

while $Z = -\mu_1$ along that curve is the orbit flip of the single homoclinic loops to P. □

Homoclinic bifurcations of n-homoclinic loops to P with $n > 1$ are found, for $\mu_1 > 0$ small, near the line pieces $\mathcal{H}_2, \ldots, \mathcal{H}_\infty$. Take a small neighborhood in the $(\bar{\mu}_2, \bar{\mu}_3)$ parameter plane of the union of these line pieces and cut out a small disk around the point O_{-1} where the line pieces join (corresponding to the orbit flip bifurcation to P). We may assume that the resulting region E is disjoint from the line piece $\mathcal{D}$ and from the points T and O_1, see Figure 8. Removing from E a small neighbourhood of $\mathcal{H}_1$ results in a region D as depicted in Figure 8.

Recall the rescaled interval map f given by (15). Consider f for parameters from D. Note that $f(\bar{x})$ is defined for $\bar{x} < \bar{x}_r = -\bar{\mu}_3/C$. Let $\bar{x}_l < \bar{x}_r$. Write $I = [\bar{x}_l, \bar{x}_r)$ and $I^* = I \cap f^{-1}(I)$. Observe that I^* consists of two intervals (having chosen $\bar{x}_l$ sufficiently smaller than $\bar{x}_r$). Consider $f : I^* \to I$. Since D is disjoint from $\mathcal{D}$, see Figure 8, the critical point of f (and a whole interval around that point) is not in I^* hence $|f'|$ is either close to A (on one branch) or very large (on the other branch) as $\mu_1 \to 0$. In any case, $|f'|$ is bounded away from 0 on I^*.

We extend these estimates to the rescaled return map

$$\bar{\Psi} = (f(\bar{x}), 0) + (h_1(\bar{x}, \bar{y}), h_2(\bar{x}, \bar{y})).$$

Lemma 5.3 below make this precise. The curve $\mathcal{C} = \left(\Psi^{glob}\right)^{-1}(\{z = 0\})$ in the stable manifold of P bounds the domain of definition of Ψ. In rescaled coordinates the domain of definition of $\bar{\Psi}$ is bounded by the curve $\bar{\mathcal{C}}$, which lies close to the line of constant $\bar{x}$ coordinate $\bar{x}_r = -\bar{\mu}_3/C$. Consider a box Δ bounded by $\bar{\mathcal{C}}, \{\bar{x} = \bar{x}_l\}$ and $\{\bar{y} = \pm k\}$. Write $\Delta^* = \Delta \cap \bar{\Psi}^{-1}(\Delta)$ for the set of points in Δ that are mapped into Δ by $\bar{\Psi}$ and consider $\bar{\Psi} : \Delta^* \to \Delta$.

Lemma 5.3 *Suppose $A > 1$ and $C < 0$. For $\mu_1 > 0$ small enough and parameters from D, the rescaled return map $\bar{\Psi}$ restricted to Δ admits a stable foliation.*

PROOF. The proof follows Lemma 4.2 in [21], to which we refer for some of the details. For $(\bar{\mu}_2, \bar{\mu}_3) \in D$ and μ_1 small, the domain of $\bar{\Psi}$ has two connected components, see Figure 9.

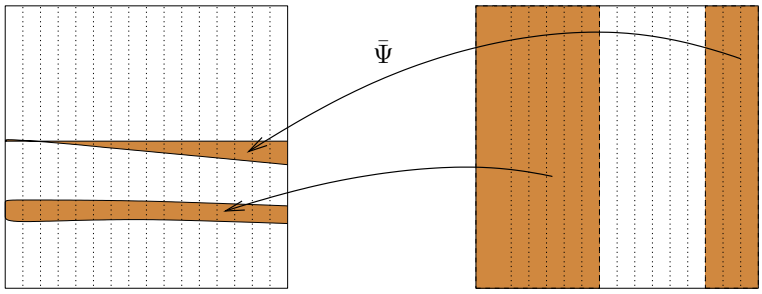

Figure 9: This picture illustrates the action of $\bar{\Psi}$ on Δ. The existence of a stable foliation for $\bar{\Psi}$ allows for a reduction to interval maps. Indicated are domain and range of $\bar{\Psi}$.

A stable foliation is obtained by iterating a trial foliation on Δ by the inverse map $\bar{\Psi}^{-1}$. Since $\bar{\Psi}^{-1}(\Delta)$ does not cover Δ, one chooses a trial foliation $\mathcal{F}$ on Δ such that the union of $\bar{\Psi}^{-1}(\mathcal{F})$ and $\mathcal{F}$ restricted to $\Delta \backslash \bar{\Psi}^{-1}(\Delta)$ provides a foliation on Δ. In particular, the vertical boundaries $\{\bar{x} = \bar{x}_l\}$ and $\bar{\mathcal{C}}$ of Δ as well as their images under $\bar{\Psi}^{-1}$ are leaves of $\mathcal{F}$. Compare also [21] and the construction of invariant foliations near hyperbolic basic sets in [22]. Iterating this procedure yields a well defined foliation in each iteration step.

The iteration of a trial foliation defines a graph transform on the space of sections in the vector bundle $\Delta \times \mathcal{L}(\mathbb{R}, \mathbb{R})$. We will show that the graph transform yields a fiber contraction, and therefore provides an invariant section $\sigma \in C^0(\Delta, \mathcal{L}(\mathbb{R}, \mathbb{R}))$. The invariant section σ defines the stable foliation by integration. Let $(\bar{x}, \bar{y}, \sigma) \mapsto (\bar{\Psi}^{-1}(\bar{x}, \bar{y}), \Sigma(\bar{x}, \bar{y}, \sigma))$ be the map induced by $\bar{\Psi}^{-1}$ on $\Delta \times \mathcal{L}(\mathbb{R}, \mathbb{R})$:

$$\Sigma(\bar{\Psi}(\bar{x}, \bar{y}), \sigma) = \frac{d(\bar{x}, \bar{y})\sigma - b(\bar{x}, \bar{y})}{-c(\bar{x}, \bar{y})\sigma + a(\bar{x}, \bar{y})},$$

where

$$D\bar{\Psi}(\bar{x}, \bar{y}) = \begin{pmatrix} a(\bar{x}, \bar{y}) & b(\bar{x}, \bar{y}) \\ c(\bar{x}, \bar{y}) & d(\bar{x}, \bar{y}) \end{pmatrix},$$

see [21]. We will demonstrate that Σ contracts distances in the last coordinate, that is

$$|\Sigma(\bar{x}, \bar{y}, \sigma_1) - \Sigma(\bar{x}, \bar{y}, \sigma_2)| \leq k\,|\sigma_1 - \sigma_2|$$

for some $k < 1$.

By Lemma 3.4, in particular the computations following its proof, we obtain the following. For the considered parameters $(\bar{\mu}_2, \bar{\mu}_3) \in D$ and $(\bar{x}, \bar{y}) \in \Delta^*$, we have that

$$|a(\bar{x}, \bar{y})| \geq L > 0 \tag{16}$$

for some $L > 0$ and moreover a is much larger than b, c, d:

$$\left|\frac{b}{a}\right|, \left|\frac{c}{a}\right|, \left|\frac{d}{a}\right| \to 0 \tag{17}$$

as $\mu_1 \to 0$. Also, a diverges as $(\bar{x}, \bar{y})$ gets close to $\bar{C}$. Away from $\bar{C}$, the partial derivative a is close to f' while the other three partial derivatives of $\bar{\Psi}$ are small.

The eigenvalues λ_1, λ_2 of $D\bar{\Psi}(\bar{x}, \bar{y})$ equal $\frac{1}{2}T \pm \frac{1}{2}T\sqrt{1 - 4D/T^2}$ with T, D denoting the trace and determinant of $D\bar{\Psi}(\bar{x}, \bar{y})$ respectively. It follows from (16), (17) that T is bounded away from 0. Because the divergence at the equilibria is negative, D and therefore also D/T^2 is small. Hence $D\bar{\Psi}(\bar{x}, \bar{y})$ has a small eigenvalue and an eigenvalue close to T, and thus bounded away from 0. (In fact, for $\bar{\mu}_1$ small, $|T|$ is larger than 1 as f' is close to 0 only very close to its critical point.) Using (17) one checks that the eigenvectors are close to the $\bar{x}$ and $\bar{y}$ axis. This is easily seen to imply that Σ defines a fiber contraction. Note that the contraction constant goes to 0 for $(\bar{x}, \bar{y}) \to \bar{C}$, making clear that Σ is continuous. Therefore Σ possesses a unique continuous fixed section $\sigma \in C^0(\Delta, \mathcal{L}(\mathbb{R}, \mathbb{R}))$. □

The following lemma implies that there are no codimension two homoclinic bifurcations of homoclinic loops to P for parameters from E. Codimension two heteroclinic bifurcations inside E occur only in $E \backslash D$, close to $\mathcal{H}_1$.

Lemma 5.4 *For $(\bar{\mu}_2, \bar{\mu}_3) \in D$ and for $\mu_1 > 0$ small enough, $X_{\bar{\mu}_2, \bar{\mu}_3}$ has no heteroclinic T-point bifurcations. For $(\bar{\mu}_2, \bar{\mu}_3) \in E$ and for $\mu_1 > 0$ small enough, $X_{\bar{\mu}_2, \bar{\mu}_3}$ has no inclination flips of homoclinic loops to P.*

Proof. For $(\bar{\mu}_2, \bar{\mu}_3) \in D$, if μ_1 is small enough, $\Psi^{glob}(\Delta)$ does not intersect $\{\bar{x} = 1\}$. This makes clear that T-points cannot occur for such parameters.

Suppose $X_{\bar{\mu}_2, \bar{\mu}_3}$ with $(\bar{\mu}_2, \bar{\mu}_3) \in D$ has a homoclinic loop γ to P. By Lemma 5.2, γ is not an orbit flip. The stable manifold of P admits a codimension one strong stable foliation. Since γ is not an orbit flip, the tangent spaces thereof provide a bundle of strong stable directions along γ. Lemma 5.3 implies that this gives a continuous bundle along $\gamma \cup \{P\}$, which is equivalent to the statement that γ is not an inclination flip.

Similar arguments show that inclination flips of homoclinic loops to P do also not occur for parameters in $E \backslash D$. For these parameters, $\Psi^{glob}(\Delta)$ may contain points in $\{\bar{x} \geq 1\}$. The set of points $\Delta^* \subset \Delta$ that return to Δ under $\bar{\Psi}$ no longer consists of two strips, so that there cannot be a stable foliation on Δ with leaves crossing Δ from $\bar{y} = -k$ to $\bar{y} = k$. The computations in the proof of Lemma 5.3 however do show the existence of an invariant bundle of stable directions over the recurrent set (note that estimates (16),(17) hold if the $\bar{x}$ coordinate of $\bar{\Psi}(\bar{x}, \bar{y})$ is away from 1 and thus for $\bar{\Psi}(\bar{x}, \bar{y}) \in \Delta$). Therefore the bundle of strong stable directions along a homoclinic loop γ to P is continuous, and inclination flips are not possible for all $(\bar{\mu}_2, \bar{\mu}_3) \in E$ and μ_1 small. □

Consider parameter values from D. Since homoclinic loops are understood via a unimodal map, for sufficiently small μ_1 they can be labeled with two symbols, say 0 and 1, in correspondence to the order found in symbolic dynamics of smooth unimodal maps. If 1 corresponds to the orientation reversing branch, then non-twisted (twisted) homoclinic loops will be those labeled with an even (odd) number of 1's.

Lemma 5.5 *There exists an infinite number of periods for which there is an odd number of non-twisted homoclinic loops to P.*

PROOF. Take a prime period p. The number of homoclinic orbits is then $(2^p - 2)/p$ but only half of those are non-twisted, i.e. $(2^{p-1} - 1)/p$. As a consequence of the Little Fermat Theorem, this number is odd. □

PROOF OF THEOREM 5.1. We employ continuation arguments as in [21]. First the accumulation of T-points is treated.

For small positive values of μ_1, the homoclinic bifurcations involving homoclinic loops to P are close to a set of line pieces $\mathcal{H}_2, \ldots, \mathcal{H}_\infty$ (compare Lemma 4.2). By Lemma's 5.2 and 5.4, for μ_1 small, there are no codimension two homoclinic bifurcations in E. Heteroclinic bifurcations in the form of T-points are not ruled out.

We do not know whether the homoclinic and heteroclinic bifurcations in E unfold generically, which would imply that codimension one homoclinic bifurcations occur along smooth curves and codimension two bifurcations at isolated points. By an arbitrary small perturbation of the family $\{X_{\bar{\mu}_2,\bar{\mu}_3}\}$, the homoclinic and heteroclinic bifurcations in E do unfold generically [21]. Perturb the family in this way for parameters near the boundary ∂E of E, leaving the vector fields unaltered away from ∂E. Observe that heteroclinic bifurcations are not altered by the perturbation, as they cannot occur on or very close to ∂E. Let ν be a homoclinic bifurcation point in ∂E, for a codimension one homoclinic bifurcation of a non-twisted homoclinic loop to P. We may further assume that ν is generically unfolding when restricting parameters to ∂E, so that there is a local curve of codimension one homoclinic bifurcations passing through ν and transverse to ∂E.

Consider a sequence $X^n_{\bar{\mu}_2,\bar{\mu}_3}$ of generic families converging to $X_{\bar{\mu}_2,\bar{\mu}_3}$ with n, equal to $X_{\bar{\mu}_2,\bar{\mu}_3}$ near ∂E. Write Γ^n for the continuation of ν for the family $X^n_{\bar{\mu}_2,\bar{\mu}_3}$ inside E. If ν gives a non-twisted homoclinic loop, then Theorem 5.2 or Lemma 5.5 from [21] implies that one of the following possibilities holds:

- Γ^n has an inclination flip in its closure (in the general theory of [21] the virtual length of the homoclinic loops along Γ^n becomes unbounded; in the present context this happens only at an inclination flip),
- Γ^n intersects ∂E twice,
- Γ^n has a heteroclinic bifurcation (a T-point) in its closure.

Without loss of generality we may assume the existence along ∂E of a unique homoclinic loop to P corresponding to each finite symbol sequence of two symbols $0, 1$. As a consequence, the second item of the list above is not possible. The first item is ruled out as well by Lemma 5.4. Since the first two items in the above list do not occur, Γ^n ends at a T-point bifurcation. Since compact parts of stable and unstable manifolds vary continuously with the vector field, an accumulation point of a sequence of T-points for $X^n_{\bar{\mu}_2,\bar{\mu}_3}$ is a T-point for $X_{\bar{\mu}_2,\bar{\mu}_3}$. This proves the statement on T-points.

The existence of inclination flips, close to O_{-1} for μ_1 small, is shown by similar means. Take a small neighborhood $\tilde{E}$ of O_{-1}. As above, $\partial\tilde{E}$ contains infinitely many homoclinic bifurcation points. Inside $\tilde{E}$, there are no heteroclinic bifurcations and the only orbit flip is O_{-1}. Continuing a n-homoclinic loop to P, it remains a n-homoclinic loop as long as it does not undergo a bifurcation. It can end at an inclination flip

of a m-homoclinic orbit only for m that divides n. By Lemma 5.5, there are infinitely many homoclinic bifurcations in $\partial\tilde{E}$ that cannot be continued back to $\partial\tilde{E}$ and therefore undergo an inclination flip bifurcation. □

As mentioned in the above proof, an arbitrary small perturbation of the family $X_{\bar{\mu}_2,\bar{\mu}_3}$, makes homoclinic and heteroclinic bifurcations unfold generically. Then codimension one homoclinic loops to P yield curves inside E, and T-points give isolated bifurcation points. Further, each finite itinerary on two symbols gives a curve of homoclinic loops ending in a T-point. The resulting picture is of a bifurcation set that is a Cantor set equal to the the closure of a set of T-points.

We end this section with remarks on the case $0 < A < 1$. The difference with the case $A > 1$ lies in the fact that $\mathcal{D}$ is accumulated by the line pieces $\mathcal{H}_i$; an invariant stable foliation for $\bar{\Psi}$ will therefore not exist for parameters near the line pieces $\mathcal{H}_i$, $i > 1$. One can however restrict parameters $(\bar{\mu}_2, \bar{\mu}_3)$ to a region $\bar{E}$ covering a finite set of line pieces $\mathcal{H}_2 \cup \ldots \cup \mathcal{H}_K$ with again a disc around O_{-1} removed. Such a region does not intersect $\mathcal{D}$ and the above reasoning for the case $A > 1$ can be applied to show the existence of infinitely many T-points inside $\bar{E}$ for μ_1 small enough.

6 Concluding remarks

The goal of this manuscript was to gain insight about the structure of homoclinic and heteroclinic bifurcations of a model capturing the relevant features of a FitzHugh-Nagumo type description of the catalytic oxidation of CO on a Pt(110) surface.

Part of the motivation for this work lies in the numerically observed two- and three-loop homoclinic orbits in [7], and further numerical and theoretical results with multi-loop pulses in [8]. In fact, it was conjectured in [7] that some numerically observed complicated behaviour of the pde could arise via the influence of unstable periodic orbits related to multi-loop pulses.

The connection with actual catalysis experiments is even more interesting. In fact, *surface* catalysis with only *one* spatial dimension may sound somewhat far-fetched. However, there exists reports of experimental setups (for other –less simple– chemical reactions) where the catalysis occurs on a ring-shaped subset of the catalytic substrate, where the width of the ring is "negligible" as compared to its length [23]. Experiments suggest the existence of one stable pulse for adequate parameter values. It would be interesting to attempt to perform the CO oxidation on a ring-shaped catalysator trying to find evidence compatible with the pulse-structure described by the present manuscript.

Also, it would be interesting to see numerical and theoretical work on the pde-side in order to establish if different stable pulses (n-loop pulses) may exist/coexist. In such a case, if the pulses would have different velocities in a 1-dimensional ring-shaped catalytic substrate, the question of "pulse collision" would become relevant. See [24] and references therein for theoretical work concerning pde stability of pulses.

References

[1] K. Krischer, M. Eiswirth, G. Ertl, Oscillatory CO oxidation on Pt(110): Modeling of temporal self-organization, *J. Chem. Phys.* **96** (1992), 9161–9172.

[2] M. Falcke, M. Bär, H. Engel, M. Eiswirth, Traveling waves in the CO oxidation on Pt(110): Theory, *J. Chem. Phys.* **97** (1992), 4555–4563.

[3] M. Bär, N. Gottschalk, M. Eiswirth, G. Ertl, Spiral waves in a surface reaction: Model calculations, *J. Chem. Physics* **100** (1994), 1202–1214

[4] M. Bär, M. Eiswirth, Turbulence due to spiral wave breakup in a continuous excitable medium, *Phys. Rev. E* **48** (1993), R1635–R1637.

[5] M. Bär, M. Hildebrand, M. Eiswirth,M. Falcke, H. Engel, M. Neufeld, Chemical turbulence and standing waves in a surface reaction model: The influence of global coupling and wave instabilities, Chaos **4** (1994), 499–508.

[6] M. Hildebrand, M. Bär, M. Eiswirth, Statistics of topological defects and spatio-temporal chaos in a reaction diffusion system, *Phys. Rev. Lett.* **75** (1995), 1503–1506.

[7] M.G. Zimmerman, S.O. Firle, M.A. Natiello, M. Hildebrand, M. Eiswirth, M. Bär, A.K. Bangia, I.G. Kevrekidis, Pulse bifurcation and transition to spatio-temporal chaos in an excitable reaction-diffusion model, *Phys. D* **110** (1997), 1–11.

[8] M.G. Zimmerman, M.A. Natiello, Homoclinic and heteroclinic bifurcations close to a twisted heteroclinic cycle, *Internat. J. Bifur. Chaos Appl. Sci. Engrg.* **8** (1998), 359–375.

[9] J. Krishnan, I.G. Kevrekidis, Ioannis G, M. Or-Guil, M.G. Zimmerman, M. Bär, Numerical bifurcation and stability analysis of solitary pulses in an excitable reaction-diffusion medium, *Comput. Methods Appl. Mech. Engrg.* **170** (1999), 253–275.

[10] B. Sandstede, A. Scheel, Gluing unstable fronts and backs together can produce stable pulses, *Nonlinearity* **13** (2000), 1465–1482.

[11] C.K.R.T. Jones, N. Kopell and R. Langer, Construction of the FitzHugh-Nagumo pulse using differential forms, in: *Patterns and Dynamics in Reactive Media*, *IMA Vol. Math. Appl.* **37**, Springer, 1991.

[12] C.K.R.T. Jones, Geometric singular perturbation theory, in: *Lecture Notes in Math.* **1609**, Springer, 1995.

[13] P. Glendinning, C. Sparrow, T-points: a codimension two heteroclinic bifurcation, *J. Statist. Phys.* **43** (1986), 479–488.

[14] Yu.S. Ilyashenko, S. Yu. Yakovenko, Finitely smooth normal forms of local families of diffeomorphisms and vector fields, *Russian Math. Surveys* **46** (1991), 1–43.

[15] V.V. Bykov, The bifurcations of separatrix contours and chaos, *Phys. D* (1993), 290–299.

[16] S.-N. Chow, B. Deng, D. Terman, The bifurcation of homoclinic and periodic orbits from two heteroclinic orbits, *SIAM J. Math. Anal.* **21** (1990), 179–204.

[17] A.J. Homburg, B. Krauskopf, Resonant homoclinic flip bifurcations, *J. Dynam. Differential Equations* **12** (2000), 807–850.

[18] B. Sandstede, *Verzweigungstheorie homokliner Verdopplungen*, PhD thesis, Free University Berlin, 1993.

[19] B. Deng, Homoclinic bifurcations with nonhyperbolic equilibria, *SIAM J. Math. Anal.* **21** (1990), 693–720.

[20] S.-N. Chow, X.-B. Lin, Bifurcation of a homoclinic orbit with a saddle-node equilibrium, *Differential Integral Equations* **3** (1990), 435–466.

[21] A.J. Homburg, H. Kokubu, V. Naudot, Homoclinic doubling cascades, *Arch. Ration. Mech. Anal.* **160** (2001), 195–243.

[22] J. Palis, F. Takens, *Hyperbolicity and sensitive chaotic dynamics at homoclinic bifurcations. Fractal dimensions and infinitely many attractors*, Cambridge University Press, 1993.

[23] J. Christoph, M. Eiswirth, N. Hartmann and R. Imbihl, I. Kevrekidis, M. Bär, Anomalous dispersion and pulse interaction in an excitable surface reaction, *Phys. Rev. Lett.* **82** (1999), 1586–1589.

[24] B. Sandstede, Stability of travelling waves, *Handbook of dynamical systems, Vol. 2*, pp. 983–1055, North-Holland, 2002.